

Available online at www.sciencedirect.com**ScienceDirect**

Procedia Engineering 101 (2015) 293 – 301

**Procedia
Engineering**

www.elsevier.com/locate/procedia

3rd International Conference on Material and Component Performance
under Variable Amplitude Loading, VAL2015

Fatigue life of welded high-strength steels under Gaussian loads

Benjamin Möller^{a,*}, Rainer Wagener^b, Jennifer Hrabowski^c,
Thomas Ummenhofer^c, Tobias Melz^{a,b}

^aTechnische Universität Darmstadt, System Reliability and Machine Acoustics SzM, Magdalenenstraße 4, 64289 Darmstadt, Germany

^bFraunhofer Institute for Structural Durability and System Reliability LBF, Bartningstraße 47, 64289 Darmstadt, Germany

^cKarlsruhe Institute of Technology, KIT Steel & Lightweight Structures, Research Center for Steel, Timber & Masonry, Otto-Ammann-Platz 1, 76131 Karlsruhe, Germany

Abstract

Within the scope of the investigation of welded high-strength steels for application in crane structures, a Gaussian-like test spectrum is derived from an analysis of recorded load time histories. In addition to stress-controlled fatigue tests under constant amplitude loading, the test spectrum is used for the experimental investigation of MAG-welded butt joints and tubular sample components under variable amplitude loading. A linear damage accumulation using Palmgren-Miner-Elementary is conservative for a damage sum of $D = 0.5$. Application of the theoretical damage sum $D_{th} = 1$ results in a closer approximation of the Gaßner-curve. For further improvement of this approximation, a rotation of the calculated Gaßner-curve, i.e. a variable damage sum, is suggested for both butt joints and sample components.

© 2015 The Authors. Published by Elsevier Ltd. This is an open access article under the CC BY-NC-ND license (<http://creativecommons.org/licenses/by-nc-nd/4.0/>).

Peer-review under responsibility of the Czech Society for Mechanics

Keywords: low cycle fatigue; high-strength fine-grained steels; welded butt joints; tubular sample components, Gaussian load spectra, linear damage accumulation, Palmgren-Miner-Elementary;

Nomenclature

CAL	constant amplitude loading	a	amplitude
D	damage sum	calc	calculated
D_{real}	real damage sum	exp	experimental
D_{spec}	damage content of the spectrum	n	number of cycles, nominal

* Corresponding author. Tel.: +49-6151-705-8443; fax: +49-6151-705-214.

E-mail address: moeller@szm.tu-darmstadt.de

D_{th}	theoretical damage sum	rot	rotated
HCF	high cycle fatigue	t	time
N, \bar{N}	number of cycles to failure (CAL and VAL)	$t_{8/5}$	cooling time from 800°C to 500°C
L_s	sequence length	$\Delta\sigma$	stress range
LCF	low cycle fatigue	$\sigma, \bar{\sigma}$	stress (CAL and VAL)
R, \bar{R}	stress ratio (CAL and VAL)		
T_N, \bar{T}_N	fatigue life scatter between $P_s = 10\%$ and 90% (CAL and VAL)		
VAL	variable amplitude loading		

1. Introduction

The typical fatigue life of crane structures is related to the low cycle fatigue (LCF) regime with a focus on critical details of MAG-welded joints. In order to achieve increasing carrying capacities and to enable lightweight design, high-strength fine-grained steels with a good weldability are applied in the design of highly loaded truck and crawler cranes. When focusing on the reserve in life time, variable amplitude loading (VAL), in addition to the LCF under constant amplitude loading (CAL), of operating truck cranes will be decisive. Therefore, service loads were analysed to derive a test spectrum and a load-time-function for investigations on butt welded high-strength steel specimens and tubular sample components.

Since 2004, truck cranes can optionally be equipped with a data logging system, recording data for the calculation of stress-time histories at highly loaded positions of the crane's telescopic boom. The sampling time varies from 5.0s to 6.6s for different datasets. The stresses were calculated from the external load with respect to geometrical configurations arising from the set-up of the crane and the extent of the telescopic boom. For two truck crane types, eighteen datasets and corresponding stress-time histories were available. The stress-time history of dataset 1 is shown in Fig. 1.

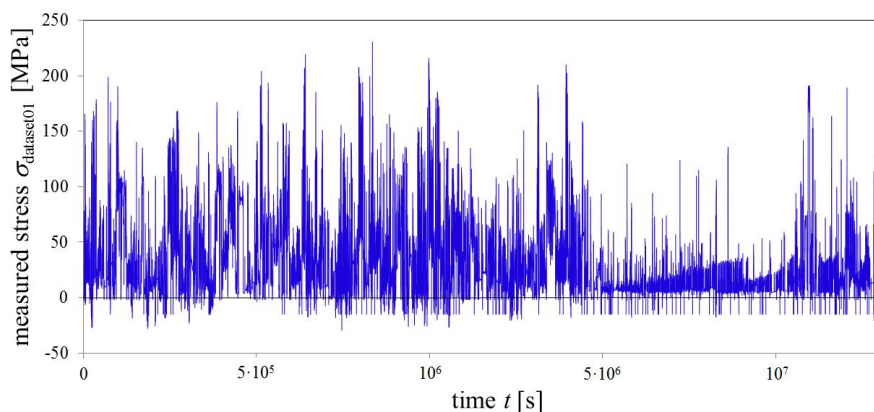


Fig. 1. Stress-time history calculated from measured data of dataset01.

For the realisation of variable loading experiments in the LCF regime, the stress-time history of each dataset was analysed by level-crossing and range-pair counting. The results of the range pair counting, shown in Fig. 2 (a), include maximum values for stress ranges $\Delta\sigma$ between 250 MPa and 350 MPa and still have a sequence length L_s larger than 10^4 cycles. Each spectrum has a Gaussian-like appearance neglecting small stresses (Fig. 2 (b)). Therefore, a mathematical Gaussian distribution was used as a basis. This is furthermore conservative towards a linear spectrum, which is recommended by [1] for service loading by superposition of measured spectra. The gradient between the two highest load levels was increased to account for special high load events (Gaussian-like spectrum), which are typical for truck cranes. In contradiction to widely-used load sequences with $L_s = 50.000$, an appropriate load sequence for the LCF was finally found using a randomly generated stress-time history with $L_s = 200$ and the maximum stress at the 113th cycle (Fig. 3). However, for a failure at 1000 to 2000 cycles, an experiment requires 5 to 10 repetitions of the sequence. This is in good agreement with a valid VAL test due to a service-like-load mixing [2, 3].

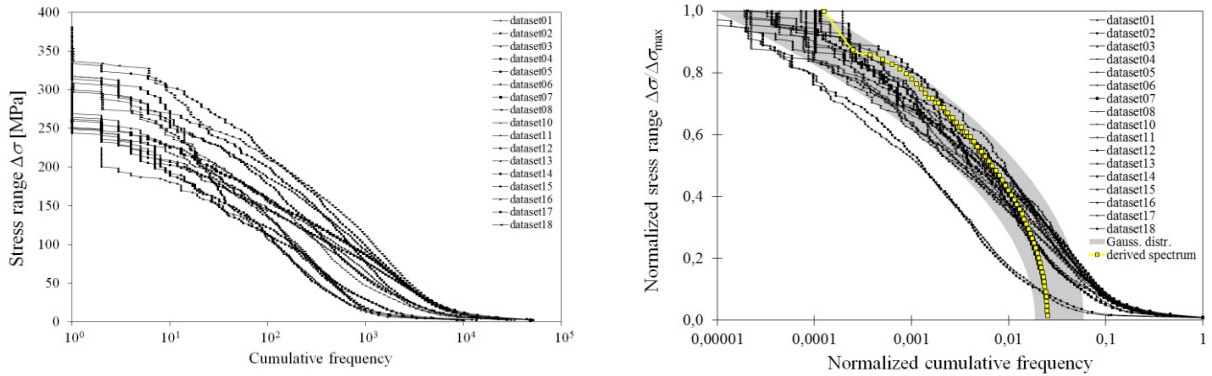


Fig. 2. (a) Range pair counting results of the datasets; (b) Normalised range pair counting results and mathematical Gaussian distribution.

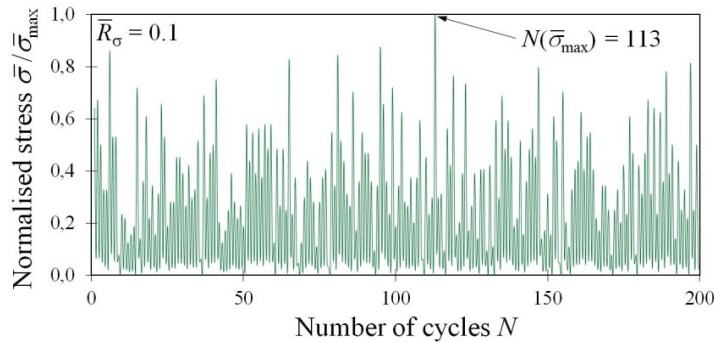


Fig. 3. Derived load sequence for stress-controlled experiments ($L_s = 200$, $\bar{R}_\sigma = 0.1$).

2. Experimental Procedure

Specimens of butt welded high-strength steel joints and sample components with tube-clevis-connections were investigated under CAL as well as VAL in the LCF regime. Stress-controlled uniaxial fatigue experiments were performed in a servo-hydraulic test rig with a maximum force of 600 kN. Both CAL and VAL have a stress ratio of $R = 0.1$ and $\bar{R} = 0.1$, respectively. The test frequency varied from 0.1 to 3.2 s^{-1} depending on the applied load level. Due to the application of welded high-strength steels in the crane industry, the focus of the experiments is set on the LCF regime, i.e. up to cycles to rupture of $5 \cdot 10^4$ or 10^5 . For the evaluation of a Wöhler- and a Gaßner-curve, the range was extended to the high cycle fatigue regime up to $2 \cdot 10^6$ by a few additional experiments.

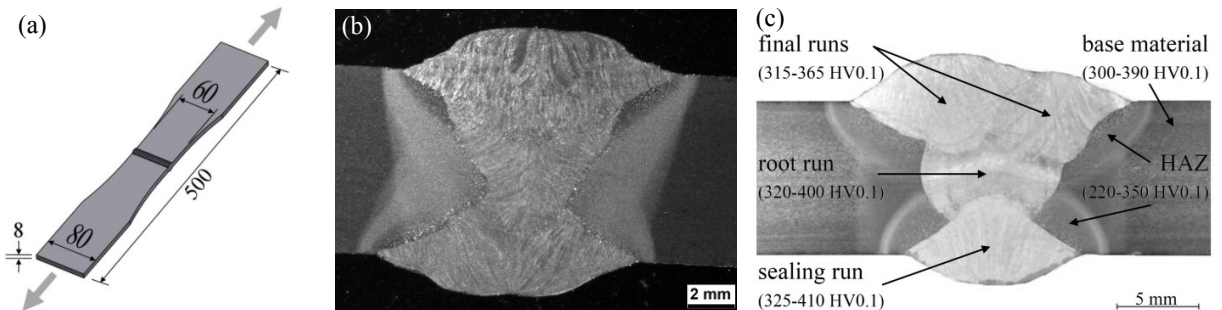


Fig. 4. (a) Specimens geometry; (b) microsection of an automated welded S960QL butt joint; (c) microsection of a manually welded S960M butt joint.

Butt welded specimens of 500 mm length (Fig. 4 (a)) and a cross section of 480 mm² were produced from the high-strength steels S960QL, S960M (2 suppliers, abbr.: suppl. 1/suppl. 2) and the ultra high-strength steel S1100QL. The specimens were removed from two 8 mm thick sheets, which had each been prepared with a 22.5° chamfer, and were joined together using a filler material of type G 89 6 M Mn4Ni2CrMo (minimum yield strength of 890 MPa). Manually welded joints of the three steel grades are compared to an automated welding in the case of the S960QL. While the S960QL, for both manual and automated processes, is welded from one side with a ground root run and a single final run (Fig. 4 (b)), the S960M and S1100QL welds have a slightly different procedure. For these two steel grades, again the root run was ground to fit in the following runs. Afterwards the sealing run was welded from the backside, finished by two overlapping final runs (Fig. 4 (c)). It should be noted that, for the S1100QL, an undermatching weld metal is used. The differences of the welding process and the transition from the base material and the heat affected zone to the weld metal can clearly be seen from the microsection of the butt weld in Fig. 4 (b) (S960QL, automated welding) and Fig. 4 (c) (S960M, suppl. 1, manual welding). A known phenomenon of MAG-welded high-strength steels is a hardness drop in the heat affected zone, below 300 HV0.1 in this particular case.

Irrespective of a manual or automated welding process for these steels, the appearance and quality in terms of strength is influenced by several factors, such as weld preparation (e.g. opening angle of the weld), welding parameters (e.g. $t_{8/5}$ time) and accuracy of the welding process. All factors individually and in combination with each other can have a significant influence on the geometrical notch of the weld toe (or the weld root for other welded details) and on the interior metallurgical notch.

Depending on the specimens, two types of sample components were produced by manual MAG-welding. For both types, a clevis (steel grade: S890QL) was welded on each end of a 700 mm long tube made of FGS100WV, which is comparable to metal sheets with a yield strength of 960 MPa. The clevis is used in the industrial products and fits to the tube dimensions with a diameter of 101.6 mm and a thickness of 5.6 mm. For the examination of the weld between tube and clevis, sample component type A is tested in this configuration. Sample component type B consists of two additional longitudinal welded elements in the middle of the tube. These are common joints to add non-load-carrying components, which are represented by small steel sheets of S355MC and S960QL.

The test rig for stress-controlled experiments on the sample components is driven by a hydraulic actuator with a maximum force of 1 MN (Fig. 5). The test frequency was varied from 0.1 to 3.2 s⁻¹ depending on the applied load level.

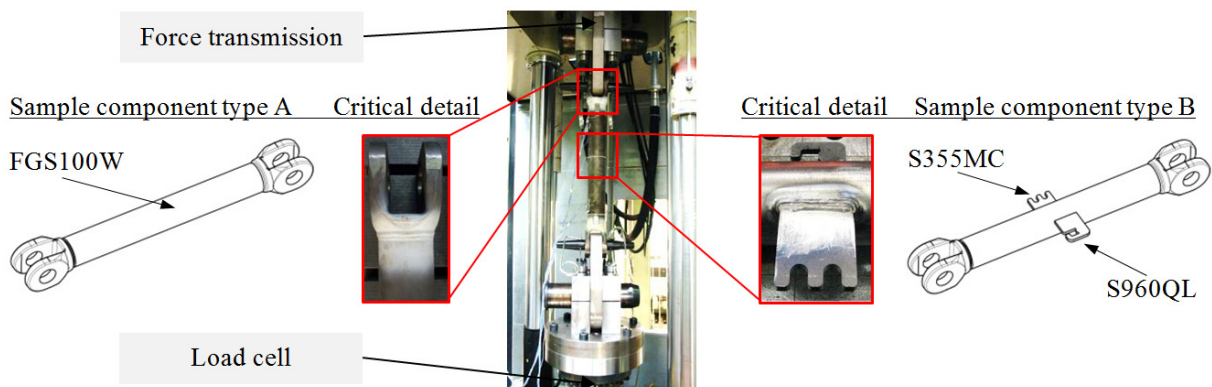


Fig. 5. Test setup for the fatigue analysis of critical details of sample components.

3. Results and discussion

In Fig. 6, experimental results of the butt welded joints are displayed in the nominal stress system for total rupture as the failure criterion. For VAL, the nominal stress amplitude is derived from the maximum load applied in each test, as suggested by [2]. A combined evaluation by linear regression of the test results under CAL (half symbols in Fig.

6) results in a Wöhler-curve with a survival probability $P_s = 50\%$. The Wöhler-curve for all steel grades, including manual (abbr.: man.) and automated (abbr.: autom.) welding, shows a slope of $k = 3.0$ and a scatter $T_\sigma = 1:1.98$. Fatigue life under VAL with a Gaussian-like distribution (filled symbols in Fig. 6) for all steels grades gives a flattened slope of $\bar{k} = 4.3$ and a reduced scatter of $\bar{T}_s = 1:1.56$. Therefore, a lifetime ratio between VAL and CAL in the HCF, e.g. at $\sigma_{a,n} = 200$ MPa, of approximately 40 can be reached, while Wöhler- and Gaßner-curve converge with increasing load level. The Wöhler-curve shows a linear relation until $\sigma_{a,n}$ reaches 300 MPa at just below 10^4 cycles, i.e. in the (lower) LCF regime. The Gaßner-curve shows a linear characteristic up to $\bar{\sigma}_{a,n} = 450$ MPa. At higher load levels, a small variation of stress ($\Delta\bar{\sigma}_{a,n} = 30$ MPa) can result in a huge difference in fatigue life, which causes a flat characteristic [4]. This range can be interpreted as a threshold into the static strength. All specimens tested under VAL finally collapsed by continuous crack growth at the maximum load of the 113th cycle.

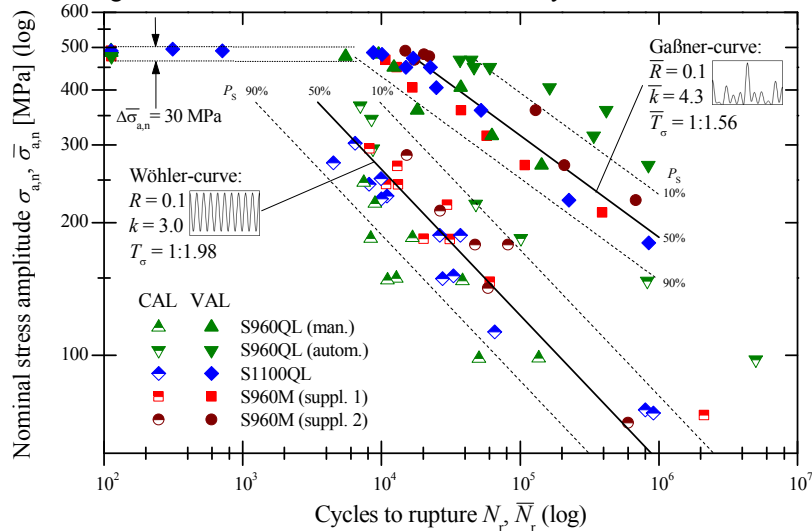


Fig. 6. Test results under CAL and VAL for butt joints.

It has already been emphasised by [5] that the sharpness of the notch at the weld toe and the quality of the welding process are major influences on the fatigue of MAG-welded high strength steels in the HCF. The results show that this is still the case in the LCF regime and under VAL. Because of the undermatching filler material, an improvement of fatigue life for the ultra high-strength steel S1100QL cannot be noted. However, variations between some of the test series can be seen, especially when fatigue results of manual and automated welded specimens are compared. Automated welded butt joints lead to an increased fatigue life under CAL as well as VAL. The reason can be found in an accurate, optimised and continuous welding process leading to few welding defects and small misalignment of the specimens in comparison to the manual process. Therefore, the applied steel grade and the arrangement of the final weld runs, explained in the microsections of Fig. 4 (a) and (b), have a minor influence.

In addition to experimental Wöhler- and Gaßner-curves, fatigue life is calculated by a linear damage accumulation according to Palmgren and Miner [6, 7] by the damage content of the spectrum

$$D_{\text{spec}} = \sum \frac{n_i}{N_i} \quad (1)$$

For welded high-strength steels, in addition to the Palmgren-Miner-Original rule, the Palmgren-Miner-Elementary method and the modification suggested by Haibach [8] were successfully applied in [9]. The choice of the modification on fatigue life has no major influence, especially for life assessment in the LCF regime. Therefore, Palmgren-Miner-Elementary ($k' = k$) is applied to the test results and the fatigue life is calculated by

$$\bar{N}_{\text{calc}} = \frac{L_s}{D_{\text{spec}}} D_{\text{real}} \quad (2)$$

In the calculation, two values for the real damage sum D_{real} have been chosen: the theoretical damage sum $D_{\text{th}} = 1$ and $D_{\text{real}} = 0.5$, which is recommended by corresponding guidelines [10, 11] for welded steels. The results of [9]

show that, for more than 90 % of the analysed data, the real damage sum is in the range between 1/3 and 3, so that, for a safe fatigue life calculation, $D_{real} = 0.3$ is recommended. In this particular investigation, an approximation of Gaßner-curves with a survival probability of $P_s = 50\%$ for butt joints and sample components without safety considerations is found.

Experimentally determined Wöhler- and Gaßner-curves as well as the calculated Gaßner-curves for each of the test series of S960QL (man.), S960QL (autom.), S960M (both suppliers) and S1100QL are shown in Fig. 7. Obviously, the calculated Gaßner-curves are not able to represent the flat characteristic of the experimental Gaßner-curve above the threshold value of ca. $\bar{\sigma}_{a,n} = 450$ MPa. The diagrams in Figure 7 show that the calculated Gaßner-curve with $D_{real} = 0.5$ underestimates the experimental Gaßner-curve below stress amplitudes of $\bar{\sigma}_{a,n} = 450$ MPa. Furthermore, the calculated Gaßner-curves with $D_{th} = 1$ intersect the experimentally determined curves with survival probability of $P_s = 90\%$ for S960QL and S1100 QL or of $P_s = 50\%$ for S960M at stress amplitudes of about $\bar{\sigma}_{a,n} = 350$ MPa.

Due to the fact that an elementary linear damage accumulation and a constant real damage sum is not able to cover the change in slope from Wöhler- to Gaßner-curve, the flattened slope of the calculated Gaßner-curve and consequently an improvement of the assessment is reached by rotation at $\bar{\sigma}_{a,n} = 350$ MPa. This corresponds to approximately 30,000 to 250,000 cycles to failure, where the LCF changes into HCF. In this investigation of MAG-welded (ultra) high-strength steels with 8 mm sheet thickness, the rotation can be expressed by increasing slope depending on the welding quality, according to Table 1. Table 2 shows slope k and \bar{k} as well as the stress amplitude at $\bar{N}_{a,n} = 2 \cdot 10^6$ cycles to failure. For welds of lower quality (manual welding), the slope is increased by 1.0. For high quality welds (i.e. automated welding), it can be increased by 0.5. The rotated, calculated Gaßner-curves improve the fatigue life assessment by linear damage accumulation.

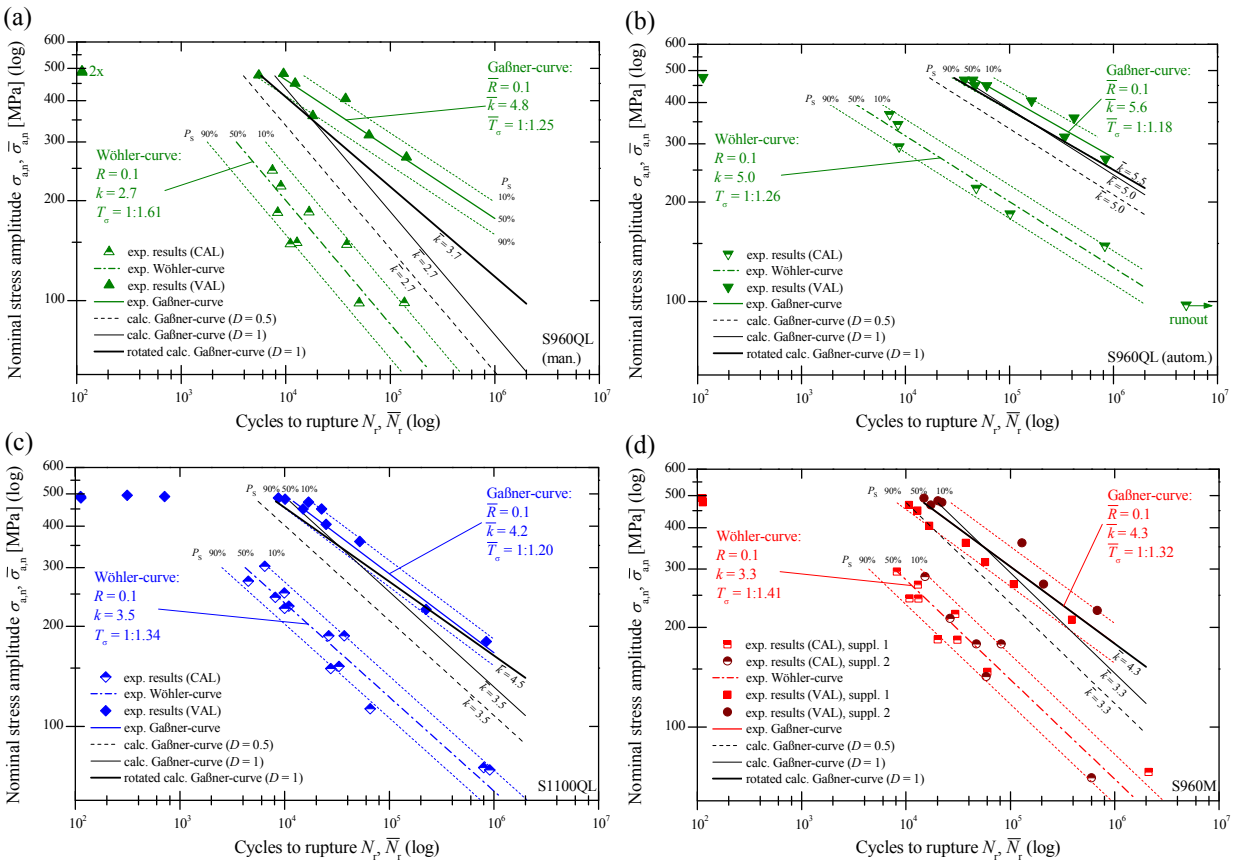


Fig. 7. Test results under CAL and VAL and calculated fatigue life for steel grades

(a) S960QL (manually welded), (b) S960QL (automated welded), (c) S1100QL and (d) S960M.

Table 1. Determination of \bar{k}_{rot} as a function of the welding quality.

Welding quality	Attribute	\bar{k}_{rot}
High	Few welding defects, angular misalignment < 2°	$\bar{k}_{calc} + 0.5$
Low	Visible welding defects, angular misalignment > 2°	$\bar{k}_{calc} + 1.0$

Table 2. Data defining experimentally evaluated and calculated fatigue life curves.

Test series (steel grade)	Wöhler-curve (exp) $\sigma_{a,n}$ ($2 \cdot 10^6$)	k	Gaßner-curve (exp) $\bar{\sigma}_{a,n}$ ($2 \cdot 10^6$)	\bar{k}	Gaßner-curve ($D = 0.5$) $\bar{\sigma}_{a,n}$ ($2 \cdot 10^6$)	\bar{k}_{calc}	Gaßner-curve ($D_{th} = 1$) $\bar{\sigma}_{a,n}$ ($2 \cdot 10^6$)	\bar{k}_{calc}	Gaßner-curve (rot) $\bar{\sigma}_{a,n}$ ($2 \cdot 10^6$)	\bar{k}_{rot}
S960QL (man.)	28 MPa	2.7	153 MPa	4.8	47 MPa	2.7	61 MPa	2.7	98 MPa	3.7
S960QL (autom.)	110 MPa	5.0	241 MPa	5.6	183 MPa	5.0	210 MPa	5.0	220 MPa	5.5
S1100QL	53 MPa	3.5	142 MPa	4.2	89 MPa	3.5	108 MPa	3.5	140 MPa	4.5
S960M	57 MPa	3.3	152 MPa	4.3	96 MPa	3.3	118 MPa	3.3	152 MPa	4.3

Finally the procedure is extended to stress-controlled test results under CAL and VAL for tubular sample components. The failure criterion for sample component type A is the total rupture of one of the welds between tube and clevis. For sample component type B, the circular weld seam at the ends of the joint elements is critical. Therefore, crack initiation can be observed at these positions (failure criterion). The experiment is finished, when the displacement sensor of the testing machine detects an increased displacement of more than 0.5 mm, so that cracks of several millimetres in length are visible and the structure would most likely collapse at the next maximum load. The experimental results as well as the calculated Gaßner-curves are shown in Fig. 8. For the determination of the experimental Gaßner-curve (in the HCF), test results below $4 \cdot 10^4$ cycles to failure have not been considered, since a non-linear relation in double-logarithmic scale can be observed. Calculated fatigue life for $D_{real} = 0.5$ is conservative with respect to survival probability of $P_s = 50\%$ for all test results. Again, the linear damage accumulation using the theoretical damage sum of $D_{th} = 1$ is a more appropriate estimation of the results, especially in combination with the suggested rotation of the curve.

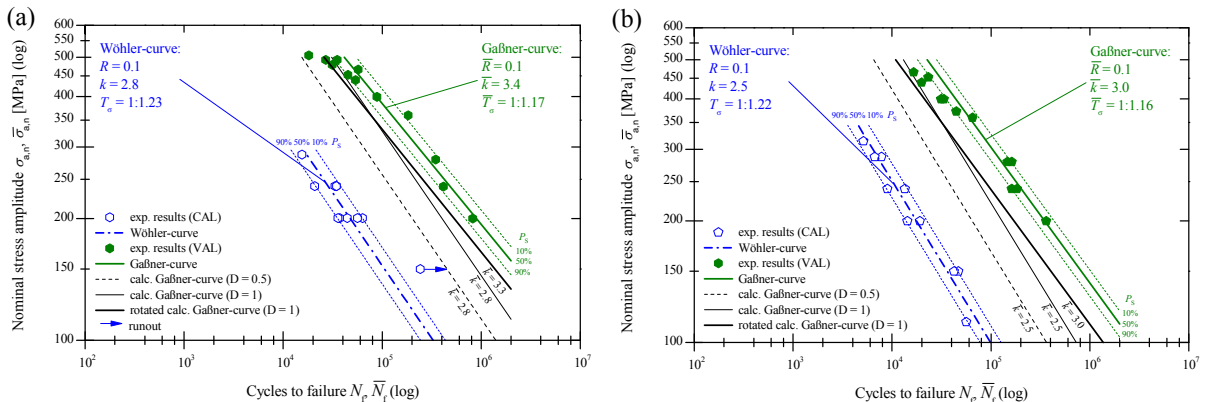


Fig. 8. Test results under CAL and VAL and calculated fatigue life for tubular sample components (a) type A, (b) type B.

4. Conclusions

Stress-controlled fatigue experiments of welded (ultra) high-strength steels under pure tensile ($R = 0.1$) CAL as well as VAL show a typical fatigue failure starting from the weld toe for MAG-welded butt joints and for longitudinal welded elements of sample component type B. Due to a comparably long crack propagation, fatigue failure can be observed at an early stage of testing and, hence, also in industrial applications. For sample component type A, crack initiation starts from the weld root between tube and clevis, so that the failure is invisible for almost the complete fatigue life. Results of the VAL tests for both sample component type A and type B tend to bend towards fewer cycles to failure in the LCF regime. However, in the design of crane structures, the influence of (non-load-carrying) welded attachments has to be considered, since sample components of type B show a decreased fatigue life in comparison to type A. Furthermore, the results of manual and automated butt joints confirm that the welding process has a major influence. Reduced fatigue life, under CAL as well as VAL, can be traced back to critical welding defects and large specimen misalignments, which should be avoided, e.g. by an automated and optimised welding process. Further improvement of the fatigue life of welded joints will be achieved by post weld treatments, but this is beyond the scope of this paper.

A linear damage accumulation according to the Palmgren-Miner rule for welded butt joints and sample components results in calculated fatigue lives and damage sums, which have values of $D = 0.5$ and higher. Therefore an approximation of the Gaßner-curve from Wöhler results is conservative for recommended damage sums of 0.3 to 0.5 from the literature. In the LCF regime, experimentally determined and calculated Gaßner-curves converge, while both lines diverge for low stress amplitudes. Within the scope of the linear damage calculation for MAG-welded butt joints, three sections of the Gaßner-curve should be separated:

- $\bar{\sigma}_{a,n} \geq 450$ MPa: threshold for a flat characteristic of the Gaßner-curve. Linear damage calculation is not able to cover this part. The elastic-plastic behaviour dominates the failure mechanisms.
- $450 \text{ MPa} > \bar{\sigma}_{a,n} \geq 350$ MPa: lower LCF regime, where calculated Gaßner-curves with $D_{th} = 1$ are a good approximation, especially when the calculated curve is rotated at $\bar{\sigma}_{a,n} = 350$ MPa.
- $\bar{\sigma}_{a,n} < 350$ MPa: transition from LCF to HCF, where calculated Gaßner-curves with $D_{th} = 1$ and $D = 0.5$ tend to be conservative.

Divergence of the Gaßner-curves is a result of the dependency from the damage mechanism, i.e. a load dependent damage sum. A practical solution can be achieved by rotating the calculated Gaßner-curve ($D_{th} = 1$), which has the same effect as a load dependent damage sum. Even though $D_{th} = 1$ is non-conservative for various welded structures, for this particular investigation it is a good choice for an approximation of a Gaßner-curve with Gaussian-like distributed spectra.

Acknowledgements

The research project „Erweiterung des örtlichen Konzeptes zur Bemessung von LCF-beanspruchten geschweißten Kranstrukturen aus hochfesten Stählen“, IGF-project-no. 17102 N, of the Research Association for Steel Application (FOSTA – Forschungsvereinigung Stahlanwendung e.V.) is funded by the AiF as part of the program for »Joint Industrial Research (IGF)« by the German Federal Ministry of Economic Affairs and Energy (BMWi) by decision of the German Bundestag.

References

- [1] M. Köhler, S. Jenne, K. Pötter, H. Zenner, Zählverfahren und Lastannahme in der Betriebsfestigkeit, Springer (2012).
- [2] C.M. Sonsino, Fatigue testing under variable amplitude loading, International Journal of Fatigue 29 (2007), pp. 1080-1089.
- [3] J. Schijve, Fatigue of Structures and Materials, AH Dordrecht: Kluwer Academic Publishers (2001).
- [4] B. Möller, R. Wagener, H. Kaufmann, H. Hanselka, J. Hrabowski, S. Herion, T. Ummerhofer, Fatigue Life Approach Method for Welded High-Strength Fine-Grained Steels in the LCF Regime, Proc. of Seventh International Conference on Low Cycle Fatigue (LCF7), Deutscher Verband für Materialforschung und -prüfung e.V. (2013), pp. 507-512.

- [5] J. Bergers, S. Herion, S., S. Höhler, C. Müller, J. Stötzel, Beurteilung des Ermüdungsverhaltens von Krankonstruktionen bei Einsatz hoch- und ultrahochfester Stähle, Stahlbau 75 (2006), Heft 11 , pp. 897-915.
- [6] A. Palmgren, Die Lebensdauer von Kugellagern, VDI-Z. 68 (1924), no. 14, pp 339-341.
- [7] M.A. Miner, Cumulative damage in fatigue, Journal of Applied Mechanics 12 (1945), no. 3, pp. A159-A164.
- [8] E. Haibach, Betriebsfestigkeit – Verfahren und Daten zur Bauteilberechnung, 1st edition, Springer (1989).
- [9] C.M. Sonsino, T. Łagoda, G. Demofonti, Damage accumulation under variable amplitude loading of welded medium- and high-strength steels, International Journal of Fatigue 26 (2004), pp. 487-495.
- [10] A. Hobbacher, Recommendations for Fatigue Design of Welded Joints and Components, International Institute of Welding (IIW), IIW document IIW-1823-07 ex XIII-2151r4-07/XV-1254r4-07 (2008), Paris.
- [11] Forschungskuratorium Maschinenbau (ed.), FKM-Richtlinie – Rechnerischer Festigkeitsnachweis für Maschinenbauteile aus Stahl, Eisenguss- und Aluminiumwerkstoffen, 6th revised edition (2012).